SCIENCE CHINA Materials ARTICLES

mater.scichina.com link.springer.com

Published online 8 May 2017 | doi: 10.1007/s40843-017-9037-1
Sci China Mater 2017, 60(7): 637–645

Controlled growth of Cu_3Se_2 nanosheets array counter electrode for quantum dots sensitized solar cell through ion exchange

Huiwen Bai[1], Ting Shen[1], Shixun Wang[1], Bo Li[1], Guozhong Cao[2*] and Jianjun Tian[1*]

ABSTRACT Copper selenide (Cu_xSe) has great potential as counter electrode for quantum dots sensitized solar cell (QDSSC) due to its excellent electrocatalytic activity and lower charge transfer resistance. A novel ion exchange method has been utilized to fabricate Cu_3Se_2 nanosheets array counter electrode. CdS layer was first deposited by sputtering and used as a template to grow compact and uniform Cu_3Se_2 film in a typical chemical bath. The morphology and thickness of the Cu_3Se_2 nanosheets were controlled by the deposition time. The final products (2h-Cu_3Se_2) showed significantly improved electrochemical catalytic activity and carrier transport property, leading to a much increased power conversion efficiency (4.01%) when compared with the CuS counter electrode CdS/CdSe QDSSC (3.21%).

Keywords: Cu_3Se_2, counter electrode, quantum dots sensitized solar cell, ion exchange

INTRODUCTION

Quantum dots sensitized solar cells (QDSSCs), a promising family of third-generation solar cells, possess significant advantages on long-term photo-stability [1], large molar extinction coefficients [2], easy tunable bandgap and the potential multiple-exciton generation [3]. With the aforementioned advantages, the theoretical maximum power conversion efficiency (PCE) could reach 44%, exceeding the Shockley-Queisser limit (33.4%) of single junction solar cells [4]. Typically, QDSSC is assembled by a transparent conductive substrate, a quantum dots loaded photoanode film, polysulfide electrolyte and a counter electrode (CE) [5]. As an important part of the photovoltaic device, CE plays a critical role in the electrons transport and oxidation of reduced ions [6], and thus is intensively investigated in recent years. In principle, high electro-catalytic and expected electrical conductivity activity are both required for an excellent CE [7].

Three categories of materials are promising counter electrode for QDSSCs, including noble metals [8], metal sulfides [9–11], and porous carbon materials [12,13]. Pt has been widely used in dye-sensitized solar cells owing to its stability and high catalytic activity for the reduction of I_3^- [14]. However, the cooperation of Pt and polysulfide electrolyte in QDSSCs is less ideal, leading to a higher overpotential and the inefficient interface catalytic activity [15]. Given that metal sulfides have excellent catalytic activity when contacting with polysulfide electrolyte, the electrode with such materials are reported to achieve the highest conversion efficiency, such as CuS, CoS and PbS [16–20]. However, since CuS can react with polysulfide electrolyte, contamination of the electrolyte and photoanode would affect the PCE and the stability of the devices [21].

Copper selenide (Cu_xSe) shows great potential in fabricating high efficiency CE for QDSSCs, due to its excellent electrocatalytic activity and lower charge transfer resistance [22,23]. Copper selenide is a family of semiconductive metal chalcogenides with different stoichiometric compositions and several crystal structures [24], such as CuSe, $CuSe_2$, Cu_2Se, Cu_3Se_2. To synthesize copper selenides with chemically stable crystal structures, several strategies have been studied, including vacuum evaporation, electrodeposition, successive ionic layer adsorption and reaction (SILAR) and chemical bath deposition (CBD) [25,26]. Although many efforts have been made on this material, the overall performance of solar cells are still unsatisfactory

[1] Institute of Advanced Materials and Technology, University of Science and Technology Beijing, Beijing 100083, China.
[2] Department of Materials Science and Engineering, University of Washington, Seattle, WA 98195-2120, USA
[*] Corresponding authors (emails: tianjianjun@mater.ustb.edu.cn (Tian J); gzcao@u.washington.edu (Cao G))

[27].

Wang *et al*. [28] reported a hot-injection method for synthesizing ultrathin $Cu_{2-x}Se$ nanosheet by cation exchange (at 220–250°C). Besides, in our previous work [29], CuS layer prepared by chemical deposition method was used as seeds for the Cu_3Se_2 crystal nucleation. However, due to the nonuniformity of CuS substrate prepared by SILAR method, the substrate was not well covered by Cu_3Se_2 nanorods, which further limited the catalytic ability of the CE. Here, Cu_xSe nanosheets array CE was synthesized *via* a novel ion exchange strategy. By controlling the processing time of chemical bath, the morphology of the Cu_xSe nanosheets was accurately regulated. X-ray diffractometry (XRD) and energy-dispersive X-ray spectroscopy (EDS) were used to reveal the crystal structure and chemical composition. When the Cu_xSe nanosheets array was used as a CE in CdS/CdSe DQSSC, the PCE was significantly improved as compared with CuS CE based solar cells, owing to much increased catalytic activity, prolonged carriers' lifetime and reduced interface recombination.

EXPERIMENTAL SECTION

Materials

Cupric acetate anhydrous ($Cu(CH_3COO)_2$, Aladdin, ≥98%), selenium powder (Alfa Aesar, 99+%), cadmium nitrate tetrahydrate ($Cd(NO_3)_2{\cdot}4H_2O$, Alfa Aesar, 98.5%), sodium bisulfite (Na_2SO_3, Alfa, 99.99%), nitrilotriacetic acid trisodium salt monohydrate ($N(CH_2CO_2Na)_3{\cdot}H_2O$, Alfa Aesar, 98%), cadmium acetate dihydrate ($(CH_3COO)_2Cd{\cdot}2H_2O$, Aladdin, 99.99%), sodium sulfide nonahydrate ($Na_2S{\cdot}9H_2O$, Aladdin, ≥98.0%), sublimed sulfur (S, Guoyao China, ≥99.5%), TiO_2 (Degussa P25), zinc nitrate hexahydrate (treatment $Zn(NO_3)_2{\cdot}6H_2O$, Aladdin, 99%) and all the chemical reagents were used as received.

Preparation of quantum dots sensitized photoanode

A layer of TiO_2 nanoparticles (P25) was covered on the clean fluorine-doped tin oxide (FTO) substrate by a doctor blade method, while the thickness was controlled at 15–20 μm. Then, the as-prepared TiO_2 films were sintered in the air at the temperature of 500°C for 30 min. For the interfacial sensitization process of CdS/CdSe quantum dots on TiO_2 photoanode films, a SILAR method was used. Specifically, TiO_2 films were firstly vertically immersed into 0.1 mol L^{-1} $Cd(NO_3)_2$ methanol solution for 1 min and rinsed with methanol, followed by vertically immersion in 0.1 mol L^{-1} Na_2S methanol solution for 1 min. The former step was repeated for 5 times. Then, a CBD method was used to prepare CdSe QDs. The TiO_2/CdS electrodes were dipped into a solution containing 0.1 mol L^{-1} $Cu(CH_3COO)_2$, 0.1 mol L^{-1} Na_2SeSO_3 and 0.15 mol L^{-1} nitrilotriacetic acid trisodium salt (NAT). Finally, the ZnS passivation layer was preparaed by SILAR method, with TiO_2/CdS/CdSe samples alternately vertically immersed into 0.1 mol L^{-1} $Zn(NO_3)_2$ and 0.1 mol L^{-1} Na_2S solutions for 1 min. This process was repeated twice. The polysulfide electrolyte was prepared as reported in our previous publication [30].

Fabrication of the Cu_3Se_2/CuS CEs based solar cells

A compact CdS layer was deposited onto the FTO glass substrate by magnetron sputtering. The sputtering power was controlled at 100 W for only 1 min. For the fabrication of the Cu_3Se_2 thin films, 0.1 mol L^{-1} of the as-prepared Na_2SeSO_3 aqueous solution, 0.1 mol L^{-1} $Cu(CH_3COO)_2$ and 0.2 mol L^{-1} nitrilotriacetic acid trisodium salt (NAT) solution were mixed with a volume ratio of 1:1:1. Then, the CdS seeds-coated FTO glasses were vertically immersed into the mixed solution at room temperature for different times. For CuS CE, a SILAR method was used. Briefly, the FTO with CdS films were first vertically immersed into 0.1 mol L^{-1} $Cu(CH_3COO)_2$ methanol solution for 1 min and rinsed with methanol, then immersed vertically into 0.1 mol L^{-1} Na_2S methanol (DI-water/methanol volume ratio 1:1) solution for 1 min. The former step was repeated for 15 times to fabricate an efficient CuS CE. At last, the quantum dots sensitized photoanode and Cu_3Se_2/CuS CEs were stacked together with the polysulfide electrolyte inserted between the two electrodes.

Characterizations

Scheme 1 shows the structure of the device, consisting of CdS/CdSe co-sensitized TiO_2 photoanode, polysulfide electrolyte and CE. The crystal structure analysis was measured by X'Pert PROS (Philips Co.) using Cu Kα radiation (1.54060 Å). The top-view and cross-section morphology of the samples were characterized by a scanning electron microscope (SEM, SU8020) and a transmission electron microscope (TEM, Tecnai F20). The current-voltage (*J*-*V*) curves of the devices were recorded under the illumination of 3A grade solar simulator (7-Star Optical Instruments Co., Ltd). Tafel polarization curves were conducted in a symmetrical dummy cell with two identical CEs using CHI660E electrochemical workstation. The active area of the QDSSCs was 0.1256 cm^2.

RESULTS AND DISCUSSION

Fig. 1 is a schematic diagram of the growing process of Cu_xSe nanosheets array. Due to the poor affinity between

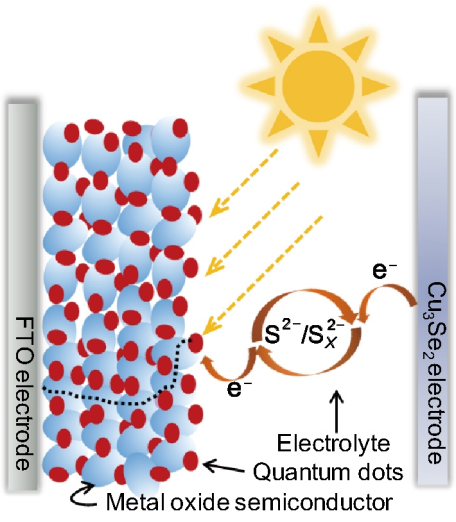

Scheme 1 Structure of the QDSSC.

Cu_3Se_2 and the surface chemical groups of FTO, it was difficult to deposit Cu_xSe nanosheets directly on the FTO substrate through a simple CBD method. However, with a thin CdS layer deposited by magnetron sputtering, the surface chemical property was significantly changed, leading to much increased adhesion sites for Cu_3Se_2. The as-prepared CdS/FTO substrate was then immersed in the Cu_x^{2+} and Se^{2-} containing precursor solution. Since the surface energy of Cu_xSe was much lower than that of CdS, CdS was believed to be dissolved by Cu^{2+} containing solution [31]. Thus, a compact Cu_xSe seeds layer was formed on the substrate after the ion exchange process. In order to make the CdS layer fully consumed, the sputtering time was strictly controlled to ensure a layer of 3–5 nm. As a result, Cu_xSe nanosheets array was grown on the substrate based on the seeds layer after a sequential CBD process.

To intuitively understand the growing process of Cu_xSe nanostructure, the surface morphology of the CEs was characterized by SEM. As shown in Fig. 2a, a compact CdS layer was deposited onto the FTO substrate. The thickness of the CdS film was 3–5 nm, which provided a uniform substrate for the formation of Cu_xSe and reduced the possibility of residual CdS. Since carrier concentration in CdS was much lower than that in Cu_xSe, the remained CdS may increase the series resistance in the CE [32]. With a typical CBD method, the Cu_x^{2+} and Se^{2-}/S^{2-} in the as-prepared solution would react with the deposited CdS and replace the crystal structure and component. The CuS film prepared with the same conditions is irregular, while many small nanosheets stacked together disorderly (Fig. 2b).

Unlike CuS nanosheets film, Cu_xSe films fabricated from the above precursor solution were well-ordered and completely covered on FTO. The morphology of the Cu_xSe films with different deposition time are exhibited in Fig. 2c–f. The vertical growth of nanosheets are conducive to the stability of Cu_xSe films and enlarges the active area of catalytic reaction on the interface of Cu_xSe films and electrolyte [33]. With such nanostructure, the possibility that Cu_xSe detached from the substrate is significantly reduced. The enlarged surface area provides more reaction sites for the reduction reaction of S_x^{2-}. The average size and surface

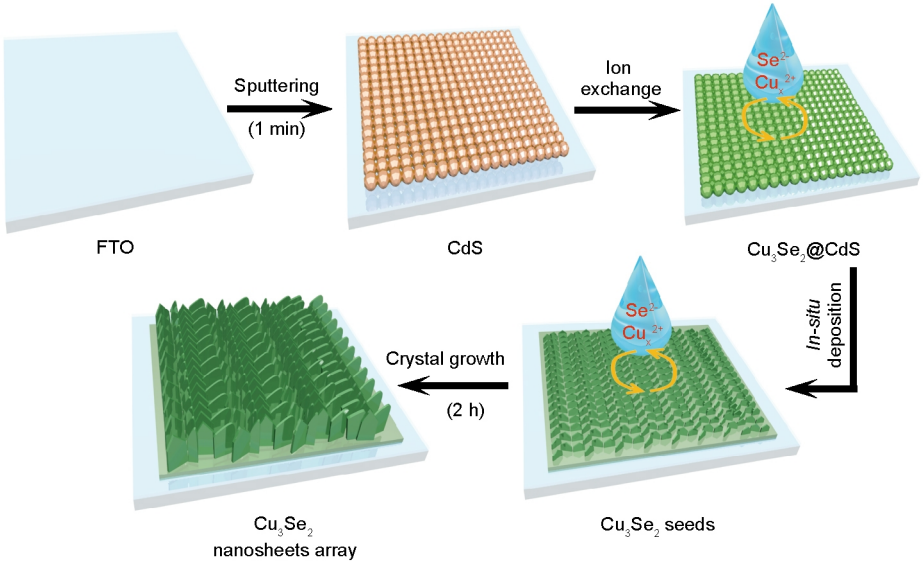

Figure 1 Schematic illustrating the growing process of Cu_xSe nanosheets array with an ion exchange.

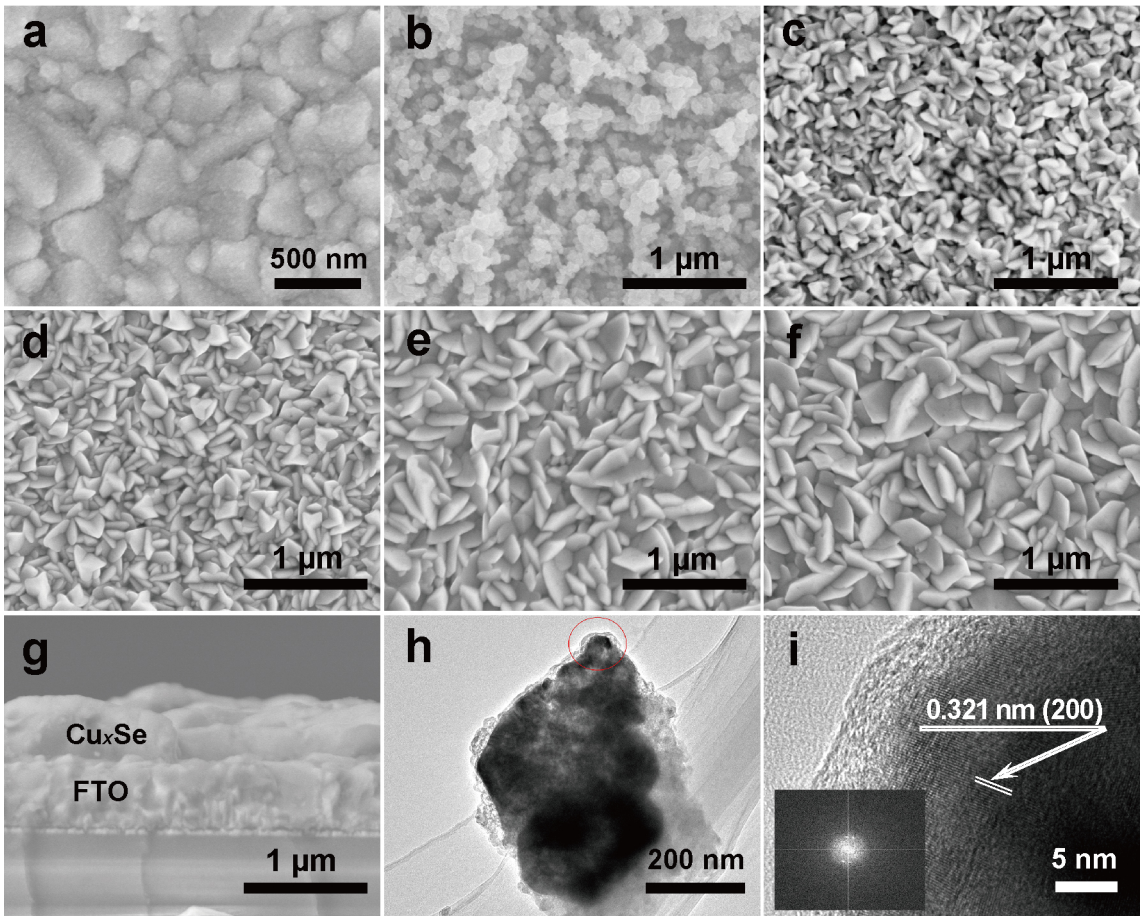

Figure 2 SEM images of different materials on FTO substrate: (a) CdS thin film, (b) CuS nanostructure, Cu_xSe nanosheets array under different grown time, (c) 0.5 h, (d) 1 h, (e) 2 h, and (f) 3 h; (g) the cross-section image of 2h-Cu_xSe film. (h) and (i) TEM images of 2h-Cu_xSe nanosheets, and the inset of (i) shows the selected area electron diffraction (SAED) pattern of Cu_xSe.

area of the Cu_xSe nanosheets is increased with the prolonged processing time, thus accelerating the depletion of Cu_xSe precursors. Since the growth rate of materials is proportional to the solute concentration [34], the dramatically declined concentration of Cu_xSe precursors (over 2 h) further limits the nanosheets growth process. The final products exhibit an average size around 300 nm. Fig. 2g shows the cross-section image of Cu_xSe film obtained from a 2 h solution reaction. The thickness of the Cu_xSe nanosheets layer is about 400 nm, while the CdS film was almost invisible revealing the occurrence of the ion exchange reaction.

Fig. 2h demonstrates the TEM image of the Cu_xSe nanosheets. The Cu_xSe nanosheets peeled from the CE are stacking in a layer or coating structure. According to the SEM image of the 2h-Cu_xSe, the average size of the nanosheets was ~300 nm and the thickness was 10–50 nm. As shown in Fig. 2i, the lattice distance is observed at 0.321 nm, corresponding to the most preferred direction of crystal orientation. However, the component of the Cu_xSe is still unclear, thus more crystallographic characterizations are needed.

Cu_xSe films were characterized by means of XRD and EDS. Fig. 3a demonstrates the XRD patterns of the Cu_xSe films with different duration of ion exchange. The XRD patterns were identical to the typical pattern of hexagonal Cu_3Se_2 (JCPDS No. 01-071-0045). The characteristic peak of (200) plane was observed at 27.9°, which corresponded to the plane with a 0.321 nm lattice distance in Fig. 2i. With increased ion exchange time, the intensity of diffraction peaks of the Cu_3Se_2 increased accordingly, while the intensity of FTO diffraction peaks decreased. Fig. 3b shows the selective ranges for (200) plane, and it can be seen that the full width at half maximum (FWHM) decreased gradually with the prolonged processing time.

Fig. 3c is the X-ray photoelectron spectroscopy (XPS)

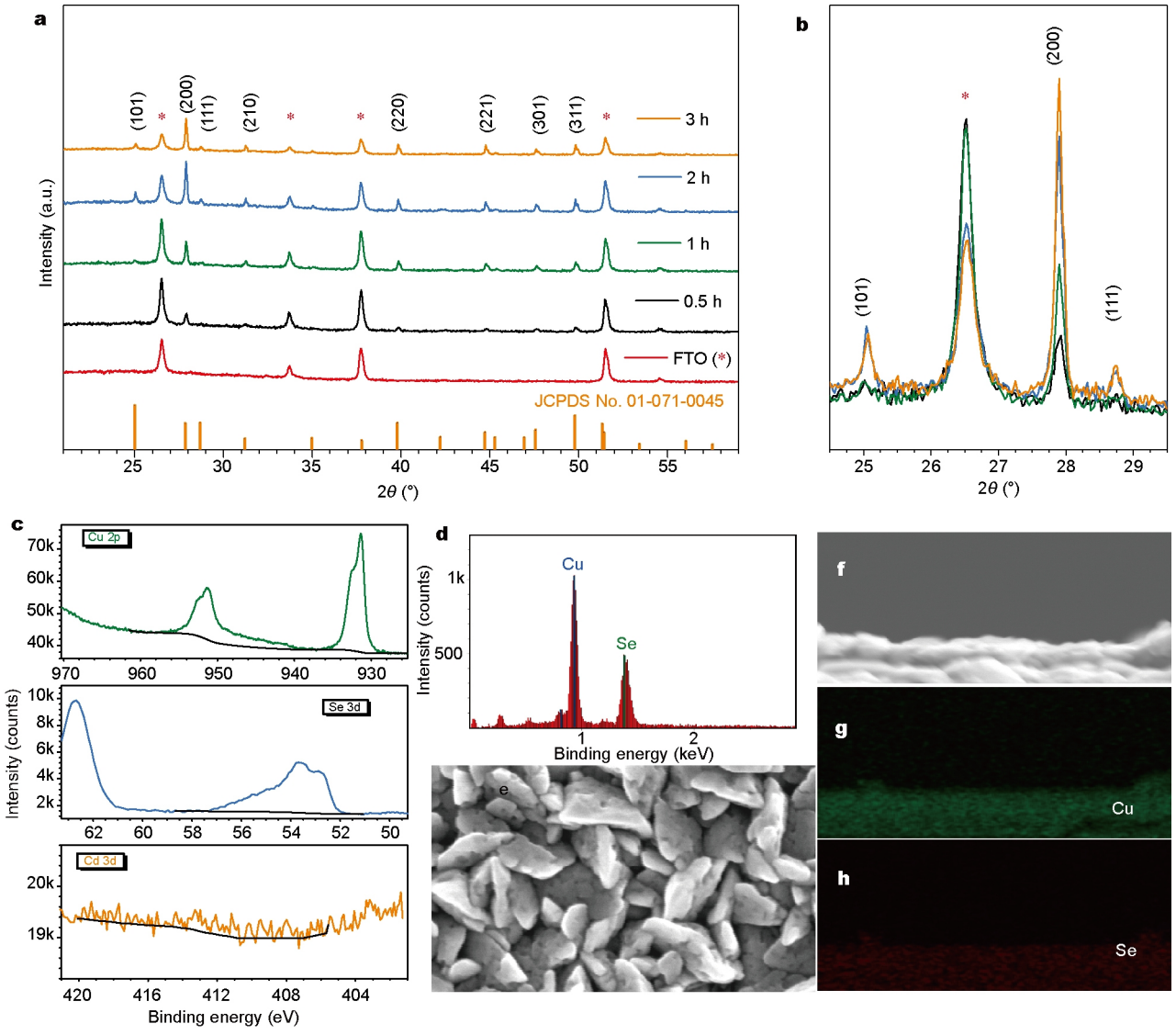

Figure 3 XRD patterns of the samples prepared from different deposition times: (a) the panorama curve from 21° to 59°, (b) selected ranges containing particular characteristics. (c) The XPS of the 2h-Cu_3Se_2 film for Cu, Se and Cd element, the blank lines are background lines. The EDS of the top-view 2h-Cu_3Se_2 film: (d) element component analysis. (e) The corresponding SEM image. The elements distribution maps: (f) cross-section SEM image, (g) Cu and (h) Se.

showing the characteristic peaks corresponding to the elements Cu, Se and Cd. The peak area ratio of Cu and Se is 17.8:12.3, nearly 3:2, which is consistent with the XRD results. Besides, there is no detectable signal of Cd element, confirming the complete phase transformation and the depletion of CdS. The EDS was also measured for further study on the reaction mechanism. The element component analysis is shown in Fig. 3d and the elements mapping of Cu_3Se_2 film is shown in Fig. 3e–g, revealing uniform and homogeneous distribution of Cu and Se.

Fig. 4a presented the photocurrent-voltage (J-V) curves of CdS/CdSe QDSSCs with various CEs, including Cu_3Se_2 and CuS films. The corresponding photovoltaic parameters, such as short-circuit current density (J_{sc}), open-circuit voltage (V_{oc}), fill factor (FF) and PCE were also summarized in Table 1. With the 2h-Cu_3Se_2 CE , the best performance of solar cells were achieved. The improved overall performance mainly originated from the increased active area, which introduced more contacting sites and electron transmission pathways [35–37]. However, the increasing of the active area might cause a serious interface charge recombination, thus in-depth declined the charge collection efficiency [38]. With the deposition time exceeding 2 h, the variation on nanosheets morphology has been a minor fac-

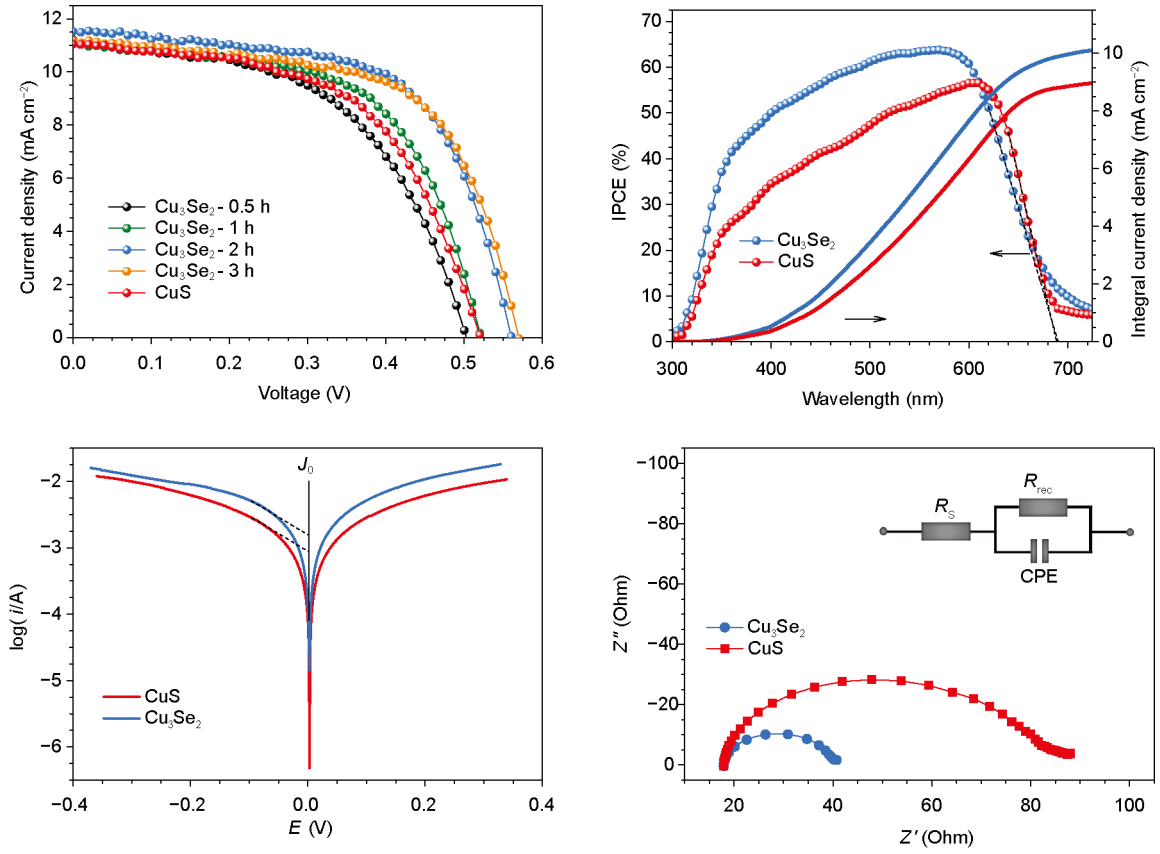

Figure 4 (a) *J-V* curves obtained from the CdS/CdSe QDSSCs based on Cu_3Se_2 CEs with different processing time and CuS CE; (b) the IPCE and integral current density of the solar cells with different CEs (Cu_3Se_2-2h and CuS); (c) Tafel polarization of the symmetrical dummy cells based on the two electrodes; (d) the impedance spectrums of the solar cells in the dark conditions.

tor when compared with the reduced charge collection efficiency. The stacking of the nanoparticles leads to the difficulty of the charge transport. Thus, the performance of solar cells based on 20 cycles CuS CE (Fig. S1) was much lower than that of the Cu_3Se_2 CE. This results indicate that the Cu_3Se_2 nanosheets array is promised to be a better electrode in CdS/CdSe QDSSCs.

Fig. 4b shows that the internal photo-to-current efficiency spectrum (IPCE) of the solar cells investigated the changes in J_{sc}. The IPCE value of Cu_3Se_2 based solar cell was increased on the full light harvesting ranges of CdS/CdSe quantum dots [39], from 300 to 687 nm. The integral current density was improved from 9.02 to 10.21 mA cm^{-2} [40], which was basically matched with the J_{sc}. Due to the limitation of our facility, the IPCE was not zero for photon energies below bandgap, while the integral current density was slightly lower than the J_{sc}.

Tafel polarization curves were also measured to demonstrate the influence of CE material on the interface properties (Fig. 4c). From the curves, the information of interfacial charge-transfer in the S^{2-}/S_n^{2-} oxidation/reduction process is revealed. The exchange current density (J_0) of Cu_3Se_2 CE calculated from the Tafel polarization curves is greater than that of CuS CE. A higher J_0 represents a lower activation energy that is needed by the reduction process of S^{2-}/S_n^{2-}, which immediately determines the electrocatalytic activity of the CEs [41]. Thus, the charge transfer property and electrocatalytic activity of Cu_3Se_2 are better than that of CuS prepared under the same condition.

Electrochemical impedance spectroscopy (EIS) was another method that can be employed to monitor the variations on the CE/electrolyte interface [38]. As shown in Fig. 4d, the impedance spectrum can be simulated into three components: series resistance (R_S), charge transfer resistance (R_{CT}) and constant phase element (CPE) [42]. R_S is related to the resistance of the electrode and external circuit, while R_{CT} is assigned to the Nernst diffusion impedance within the electrolyte [43]. The R_{CT} values of the Cu_3Se_2 and CuS based solar cells were 22.92 and 68.59 Ω, respectively. The reduced R_{CT} of Cu_3Se_2 often resulted in high catalytic

Table 1 Photovoltaic parameters calculated from the *J-V* curves of the CdS/CdSe QDSSCs based on Cu_3Se_2 and CuS CEs (the data are the average values)

Samples	J_{sc} (mA cm^{-2})	V_{oc} (V)	FF	η (%)
Cu_3Se_2-0.5 h	11.21	0.503	0.527	2.81±0.26
Cu_3Se_2-1 h	11.05	0.521	0.596	3.41±0.04
Cu_3Se_2-2 h	11.52	0.560	0.621	3.99±0.02
Cu_3Se_2-3 h	11.18	0.570	0.620	3.89±0.04
CuS	11.05	0.521	0.558	3.18±0.01

ability, which was beneficial to the V_{oc}, FF and J_{sc}.

CONCLUSIONS

A novel ion exchange method was used to fabricate compact and uniform Cu_3Se_2 nanosheets array CE for quantum dots solar cells. With the processing of CBD, the CdS layer was dissolved in the Cu_3Se_2 precursor solution gradually, while Cu^{2+} and Se^{2-} were deposited onto the surface of the substrate. The morphology of the Cu_3Se_2 nanosheets could be controlled by the deposition time. With a 2 h solution processing, the best catalytic performance of the CE was obtained. Compared with CuS electrode, Cu_3Se_2 nanosheets CE possessed lower electrocatalytic active energy, less recombination sites and longer carriers' lifetime. The CdS/CdSe QDSSCs based on Cu_3Se_2 nanosheets array CE exhibited a 4.01% PCE, better than that of the CuS based solar cells (3.21%).

Received 2 March 2017; accepted 17 April 2017; published online 8 May 2017

1 Chuang CHM, Brown PR, Bulović V, *et al.* Improved performance and stability in quantum dot solar cells through band alignment engineering. Nat Mater, 2014, 13: 796–801
2 Sargent EH. Colloidal quantum dot solar cells. Nat Photon, 2012, 6: 133–135
3 Beard MC. Multiple exciton generation in semiconductor quantum dots. J Phys Chem Lett, 2011, 2: 1282–1288
4 Alharbi FH, Kais S. Theoretical limits of photovoltaics efficiency and possible improvements by intuitive approaches learned from photosynthesis and quantum coherence. Renew Sustain Energ Rev, 2015, 43: 1073–1089
5 Tian J, Zhang Q, Uchaker E, *et al.* Architectured ZnO photoelectrode for high efficiency quantum dot sensitized solar cells. Energ Environ Sci, 2013, 6: 3542–3547
6 Hwang I, Yong K. Counter electrodes for quantum-dot-sensitized solar cells. CHEMELECTROCHEM, 2015, 2: 634–653
7 Liu T, Hou J, Wang B, *et al.* Correlation between the in-plain substrate strain and electrocatalytic activity of strontium ruthenate thin films in dye-sensitized solar cells. J Mater Chem A, 2016, 4: 10794–10800
8 Kumar PN, Narayanan R, Deepa M, *et al.* Au@poly(acrylic acid) plasmons and C_{60} improve the light harvesting capability of a TiO_2/CdS/CdSeS photoanode. J Mater Chem A, 2014, 2: 9771–9783
9 Ke W, Fang G, Lei H, *et al.* An efficient and transparent copper sulfide nanosheet film counter electrode for bifacial quantum dot-sensitized solar cells. J Power Sources, 2014, 248: 809–815
10 Lei H, Fang G, Cheng F, *et al.* Enhanced efficiency in organic solar cells *via in situ* fabricated p-type copper sulfide as the hole transporting layer. Sol Energ Mater Sol Cells, 2014, 128: 77–84
11 Gopi CVVM, Venkata-Haritha M, Lee YS, *et al.* ZnO nanorods decorated with metal sulfides as stable and efficient counter-electrode materials for high-efficiency quantum dot-sensitized solar cells. J Mater Chem A, 2016, 4: 8161–8171
12 Du Z, Pan Z, Fabregat-Santiago F, *et al.* Carbon counter-electrode-based quantum-dot-sensitized solar cells with certified efficiency exceeding 11%. J Phys Chem Lett, 2016, 7: 3103–3111
13 Guo W, Chen C, Ye M, *et al.* Carbon fiber/Co_9S_8 nanotube arrays hybrid structures for flexible quantum dot-sensitized solar cells. Nanoscale, 2014, 6: 3656–3663
14 Grätzel M. Recent advances in sensitized mesoscopic solar cells. Acc Chem Res, 2009, 42: 1788–1798
15 Chen H, Zhu L, Liu H, *et al.* Efficient iron sulfide counter electrode for quantum dots-sensitized solar cells. J Power Sources, 2014, 245: 406–410
16 Zhao K, Pan Z, Mora-Seró I, *et al.* Boosting power conversion efficiencies of quantum-dot-sensitized solar cells beyond 8% by recombination control. J Am Chem Soc, 2015, 137: 5602–5609
17 Du J, Du Z, Hu JS, *et al.* Zn–Cu–In–Se quantum dot solar cells with a certified power conversion efficiency of 11.6%. J Am Chem Soc, 2016, 138: 4201–4209
18 Yang Z, Chen CY, Liu CW, *et al.* Quantum dot-sensitized solar cells featuring CuS/CoS electrodes provide 4.1% efficiency. Adv Energ Mater, 2011, 1: 259–264
19 Tachan Z, Shalom M, Hod I, *et al.* PbS as a highly catalytic counter electrode for polysulfide-based quantum dot solar cells. J Phys Chem C, 2011, 115: 6162–6166
20 Lei H, Qin P, Ke W, *et al.* Performance enhancement of polymer solar cells with high work function CuS modified ITO as anodes. Org Electron, 2015, 22: 173–179
21 Radich JG, Dwyer R, Kamat PV. Cu_2S reduced graphene oxide composite for high-efficiency quantum dot solar cells. overcoming the redox limitations of S_2^-/S_n^{2-} at the counter electrode. J Phys Chem Lett, 2011, 2: 2453–2460
22 Zhang H, Wang C, Peng W, *et al.* Quantum dot sensitized solar cells with efficiency up to 8.7% based on heavily copper-deficient copper selenide counter electrode. Nano Energ, 2016, 23: 60–69
23 Liu F, Zhu J, Hu L, *et al.* Low-temperature, solution-deposited metal chalcogenide films as highly efficient counter electrodes for sensitized solar cells. J Mater Chem A, 2015, 3: 6315–6323
24 Danilkin SA, Skomorokhov AN, Hoser A, *et al.* Crystal structure and lattice dynamics of superionic copper selenide $Cu_{2-\delta}Se$. J Alloys Compd, 2003, 361: 57–61

25 Saldanha PL, Brescia R, Prato M, *et al.* Generalized one-pot synthesis of copper sulfide, selenide-sulfide, and telluride-sulfide nanoparticles. Chem Mater, 2014, 26: 1442–1449
26 Xiao G, Ning J, Liu Z, *et al.* Solution synthesis of copper selenide nanocrystals and their electrical transport properties. CrystEngComm, 2012, 14: 2139–2144
27 Eskandari M, Ahmadi V. Copper selenide as a new counter electrode for zinc oxide nanorod based quantum dot solar cells. Mater Lett, 2015, 142: 308–311
28 Wang Y, Zhukovskyi M, Tongying P, *et al.* Synthesis of ultrathin and thickness-controlled $Cu_{2-x}Se$ nanosheets via cation exchange. J Phys Chem Lett, 2014, 5: 3608–3613
29 Wang S, Shen T, Bai H, *et al.* Cu_3Se_2 nanostructure as a counter electrode for high efficiency quantum dot-sensitized solar cells. J Mater Chem C, 2016, 4: 8020–8026
30 Tian J, Lv L, Fei C, *et al.* A highly efficient (>6%) $Cd_{1-x}Mn_xSe$ quantum dot sensitized solar cell. J Mater Chem A, 2014, 2: 19653–19659
31 Shen T, Bian L, Li B, *et al.* A structure of CdS/Cu_xS quantum dots sensitized solar cells. Appl Phys Lett, 2016, 108: 213901
32 Thirumavalavana S, Mani K, Sagadevan SS, *et al.* Studies on Hall effect and DC conductivity measurements of semiconductor thin films prepared by chemical bath deposition (CBD) method. J Nano Electron Phys, 2015, 7: 04024
33 Jiang S, Yin X, Zhang J, *et al.* Vertical ultrathin MoS_2 nanosheets on a flexible substrate as an efficient counter electrode for dye-sensitized solar cells. Nanoscale, 2015, 7: 10459–10464
34 Wang Y, Tian J, Fei C, *et al.* Microwave-assisted synthesis of SnO_2 nanosheets photoanodes for dye-sensitized solar cells. J Phys Chem C, 2014, 118: 25931–25938
35 Xu Y, Zhou M, Lei Y. Nanoarchitectured array electrodes for rechargeable lithium- and sodium-ion batteries. Adv Energ Mater, 2016, 6: 1502514
36 Tian J, Uchaker E, Zhang Q, *et al.* Hierarchically structured ZnO nanorods–nanosheets for improved quantum-dot-sensitized solar cells. ACS Appl Mater Interfaces, 2014, 6: 4466–4472
37 Li LB, Wu WQ, Rao HS, *et al.* Hierarchical ZnO nanorod-on-nanosheet arrays electrodes for efficient CdSe quantum dot-sensitized solar cells. Sci China Mater, 2016, 59: 807–816
38 Basu K, Benetti D, Zhao H, *et al.* Enhanced photovoltaic properties in dye sensitized solar cells by surface treatment of SnO_2 photoanodes. Sci Rep, 2016, 6: 23312
39 Shen T, Tian J, Li B, *et al.* Ultrathin ALD coating on TiO_2 photoanodes with enhanced quantum dot loading and charge collection in quantum dots sensitized solar cells. Sci China Mater, 2016, 59: 833–841
40 Fei C, Guo L, Li B, *et al.* Controlled growth of textured perovskite films towards high performance solar cells. Nano Energ, 2016, 27: 17–26
41 Soo Kang J, Park MA, Kim JY, *et al.* Reactively sputtered nickel nitride as electrocatalytic counter electrode for dye- and quantum dot-sensitized solar cells. Sci Rep, 2015, 5: 10450
42 Gao R, Liang Z, Tian J, *et al.* ZnO nanocrystallite aggregates synthesized through interface precipitation for dye-sensitized solar cells. Nano Energ, 2013, 2: 40–48
43 Shi Z, Deng K, Li L. Pt-free and efficient counter electrode with nanostructured $CoNi_2S_4$ for dye-sensitized solar cells. Sci Rep, 2015, 5: 9317

Acknowledgments This work was supported by the National Natural Science Foundation of China (51374029 and 51611130063), Fundamental Research Funds for the Central Universities (FRF-BD-16-012A), and 111 Project (B17003).

Author contributions Bai H wrote this manuscript under the guidance of Cao G and Tian J. All authors contributed to the general discussion.

Conflict of interest The authors declare that they have no conflict of interest.

Huiwen Bai is currently pursuing her Master degree in the University of Science and Technology Beijing. Her research is focused on the synthesis of quantum dots and counter electrode materials for QDSCs.

Guozhong Cao is a Boeing Steiner Professor of Materials Science and Engineering, Professor of Chemical Engineering, and Adjunct Professor of Mechanical Engineering at the University of Washington. He has published over 400 papers, 8 books and 4 proceedings. His recent research is mainly focused on solar cells, lithium-ion batteries, supercapacitors, and hydrogen storage.

Jianjun Tian is a professor in Advanced Material and Technology Institute, University of Science and Technology Beijing. His current research is focused on QDSCs and perovskite solar cells.

离子交换法调控生长的用作量子点太阳电池对电极的Cu_3Se_2纳米片阵列

白慧文[1], 沈婷[1], 王世勋[1], 李波[1], 曹国忠[2*], 田建军[1*]

摘要 硒化铜(Cu_xSe)凭借优良的电催化活性和较低的电荷转移电阻, 在量子点敏化太阳电池(QDSSC)对电极方面表现出了巨大的潜力. 本研究采用一种新的离子交换方法制备了Cu_3Se_2纳米片阵列. 通过溅射沉积CdS层作为模板, 在化学浴中生长出均匀和高覆盖度的Cu_3Se_2薄膜, Cu_3Se_2纳米片的形貌和厚度由沉积时间控制, 最终产物(2h-Cu_3Se_2)显著改善了电化学催化活性和载流子传输性能, 相比较于CuS为对电极的CdS / CdSe量子点敏化太阳能电池, 其光伏性能由3.21%提升至4.01%.